Enhanced organic degradation and biogas production of domestic wastewater at psychrophilic temperature through submerged granular anaerobic membrane bioreactor for energy-positive treatment

Lucie Sanchez, Morgane Carrier, Jim Cartier, Christophe Charmette, Marc Heran, Geoffroy Lesage, Jean-Philippe J.-P. Steyer

Enhanced organic degradation and biogas production of domestic wastewater at psychrophilic temperature through submerged granular anaerobic membrane bioreactor for energy-positive treatment

Lucie Sanchez[a], Morgane Carrier[a], Jim Cartier[a], Christophe Charmette[a], Marc Heran[a], Jean-Philippe Steyer[b], Geoffroy Lesage[a]

[a] Institut Européen des Membranes (IEM), Université de Montpellier, CNRS, ENSCM, Montpellier, France

[b] INRAE, Univ Montpellier, LBE, Narbonne, France

ABSTRACT

This study deals with the conversion of organic matter into methane at ambient temperature, during anaerobic digestion of domestic wastewater combined with a submerged ultrafiltration membrane with no gas-sparging. A one-stage submerged granular anaerobic membrane bioreactor (G-AnMBR) and a control anaerobic digester (UASB type) were operated during four months, after 500 days of biomass acclimatization to psychrophilic and low loading rate conditions. Membrane barrier led to the retention of biomass, suspended solids and dissolved and colloidal organic matter which greatly enhanced total COD (tCOD) removal (92.3%) and COD to methane conversion (84.7% of tCOD converted into dissolved and gaseous CH4). G-AnMBR overcame the usual long start-up period and led to a higher sludge heterogeneity, without altering the granular biomass activity. The feasibility of the G-AnMBR without gas-sparging was also assessed and the net positive energy balance was estimated around +0.58 kWh.m^{-3}.

KEYWORDS

ultrafiltration; anaerobic digestion; granular biomass; low-strength wastewater; energy recovery.

1. Introduction

For the last decade, large attention has been given to establish a balance between human well-being and environment preservation. In this way, intensive resource use is switching into a circular economy approach, based on the reuse and recycling of resources. For those reasons, wastewater is not only considered as an alternative source of water but also as a source of nutrients, minerals and energy (Batstone and Virdis, 2014). In this sustainable development context, anaerobic digestion (AD) presents many advantages over conventional activated sludge (CAS) processes for domestic wastewater treatment (DWWT) since (i) it does not require aeration, which decreases energy-demand and associated costs, (ii) it produces a smaller amount of sludge, begetting less sludge processing and disposal difficulties and costs, and (iii) it converts organic matter into energy in the form of methane (van Lier et al., 2008). Recent studies have evaluated a world domestic wastewater production of 359.10^9 $m^3.year^{-1}$ (Jones et al., 2021) with a chemical oxygen demand (COD) concentration between 210 and 740 $mgCOD.L^{-1}$ (Srinivasa Raghavan et al., 2017). Based on the theoretical conversion rate of 0.35 m^3-$CH_4.kgCOD^{-1}$ and the calorific energy of methane of 35.9 kJ.L-CH_4^{-1}, it appears that 263-903 $TWh.year^{-1}$ of energy could be recoverable from wastewater through AD, that means up to a third of the electricity consumed by the European Union. It highlights the high bioenergy potential of anaerobic domestic wastewater treatment as an alternative through fossil consumption and an ease on energy insecurity (Chen et al., 2016).

However, the feasibility of the dominant anaerobic technologies (i.e. upflow anaerobic sludge blanket (UASB) and expended granular sludge bed (EGSB)) for domestic wastewater is challenged by low influent substrate concentration, huge wastewater quantities and

psychrophilic temperature (≤25 °C) (Maaz et al., 2019; Vinardell et al., 2020). Thus, even if the UASB are applied to domestic wastewater in some tropical countries (i.e. Brazil, India, Colombia), UASB treatment plants still exhibit substandard effluent quality discharge and poor biogas production (Chernicharo et al., 2015; Srinivasa Raghavan et al., 2017; Kong et al., 2021b). Anaerobic membrane bioreactor (AnMBR) has been found to overcome UASB weakness since it enables to operate at high sludge retention times (SRT) and short hydraulic retention times (HRT). Therefore, even at high volumetric flow rates, ultrafiltration membrane rejection ensures the growth of slow anaerobic communities and, as a result, improves the conversion of organic matter into methane energy content (Ji et al., 2021; Robles et al., 2018). Plus, the membrane unit performs pathogens rejection and could improve organic micropollutants removal (Robles et al., 2018). Since no nitrogen and phosphorus degradation is expected from AD, the nutrients-rich effluent could be viewed as a valuable product suitable for reuse applications (e.g. fertilizer, irrigation) (Maaz et al., 2019). Thus, AnMBR has the potential to produce a relevant effluent for water reuse while performing a positive net energy balance (NEB) (Robles et al., 2018; Vinardell et al., 2020). Nevertheless, dissolved methane and membrane fouling are key issues for full-scale implementation (Maaz et al., 2019). The loss of energy, in the form of dissolved methane within the effluent, is a well-known issue for anaerobic wastewater treatment at psychrophilic temperature, due to the methane solubility increase with a decrease in temperature and the entrapment of biogas inside the sludge bed. Typical dissolved methane concentration ranges between 10 and 25 mg-CH_4.L^{-1} and up to 100% of the total produced methane could be lost in the effluent (Sohaib et al., 2022). Fortunately, developing processes, such as degassing membrane, air stripping oxidation and engineered methanotrophic community in photogranules, have proven their ability to remove most of the dissolved methane which is attractive for energy recovery

and/or to prevent greenhouses gas (GHG) emissions (Robles et al., 2018; Safitri et al., 2021; Sohaib et al., 2022).

As for now, the major constraint to achieve energy-positive AnMBR is membrane fouling (Maaz et al., 2019). Submerged membrane configuration presents the advantages to be less energy-consuming for suction and more compact (Liao et al., 2006), nonetheless, it implies that gas-sparging is the easiest way to mitigate membrane fouling. Studies based on AnMBR energy demand stated that more than 70% of the energy consumption owed to gas-sparging for fouling control (Batstone and Virdis, 2014; Smith et al., 2014). To cut the high operational cost, several research have been undertaken to understand, limit and control membrane fouling (Robles et al., 2018).

Granular anaerobic membrane bioreactor (G-AnMBR), a hybrid biotechnology that incorporates AnMBR and granular biomass, has raised attention as a sustainable AD process (Vinardell et al., 2020). Granular sludge presents a great advantage over flocculent sludge for its (i) high settling capacity, (ii) well-balanced bacteria consortia, (iii) compact and dense biomass structure and (iv) high-strength to loading rates and toxics shocks (van Lier et al., 2008). As a result, previous studies stated that granular biomass technology increases biological removal efficiencies, methane production yield and membrane mitigation (Deng et al., 2020; Iorhemen et al., 2017). Therefore, the G-AnMBR configuration could be a way to work without an energy-intensive gas-sparging fouling control strategy and could lead to a process where the energy recovery overcomes the energy consumption of the system (Smith et al., 2014).

The novelty of this research lies in the unusual G-AnMBR configuration that combines a granular biomass and a membrane submerged directly inside the sludge bed, without gas-sparging for fouling control. Hence, the objective of this paper is two-fold. First, to evaluate

and understand the impact of a submerged membrane inside a granular anaerobic digester (i.e. one-stage reactor), focusing on the treatment performances, biogas production and granular biomass behavior. Second, to study the feasibility of an efficient and positive-energy DWWT through G-AnMBR at 25°C, without gas-sparging for fouling mitigation. Therefore, a submerged G-AnMBR and an UASB, as a control reactor, have been continuously operated during four months with the same operating conditions.

2. Materials and methods

2.1 Inoculum and wastewater composition

The seed granular sludge was taken from a full-scale UASB, treating the sewage from a manufacturer of recycled paper (Saica Paper Champblain-Laveyron, France), at mesophilic temperature (35-38°C) with an organic loading rate (OLR) of 18 $kgCOD.m^{-3}.d^{-1}$. The granular biomass was gradually acclimatized to ambient temperature (25°C) and low-strength synthetic wastewater during a period of 500 days (see supplementary material). The lab-scale reactors were then inoculated with the acclimatized anaerobic granular sludge at a concentration of 70 ± 9.7 and 66 ± 9.2 gTS/L for the UASB and G-AnMBR respectively. The influent composition was adjusted from Layer et al. (2019) with a C:N:P ratio of 100:1:0.2 and a COD concentration corresponding to low-strength wastewater (WW). This complex synthetic WW was chosen for its capacity to lead to the development of granular sludge with the same characteristics to those fed with raw WW (Layer et al., 2019). The synthetic WW was prepared weekly and stored under mixing at 4°C. The influent was characterized by total COD (tCOD) of 274 ± 76 $mgCOD.L^{-1}$, soluble COD (sCOD) of 224 ± 65 $mgCOD.L^{-1}$, particulate COD (pCOD) of 50 ± 27 $mgCOD.L^{-1}$, dissolved organic carbon (DOC) of 98 ± 30 $mgC.L^{-1}$, volatile fatty acids (VFA) of 130 ± 32 $mgCOD.L^{-1}$, ammonia (NH_4^+-N) of 3.8 ± 1.6 $mgN.L^{-1}$, nitrite (NO_2^--N) of 0.2 ± 0.1 $mgN.L^{-1}$, orthophosphate (PO_4^{3-}-P) of 0.5 ± 0.2 $mgP.L^{-}$

[1], sulfate (SO_4^{2-}—S) of 11.0 ± 0.5 mgS.L^{-1}. pCOD and VFA represent about 20% and 50% respectively of the influent tCOD.

2.2 Experimental set-up and operating conditions

Two granular anaerobic reactors, namely G-AnMBR and UASB (as a control reactor), were continuously operated in parallel during 120 days. The two experimental lab-scale reactors consisted of parallelepiped-shaped tanks with equal working volume of 6.2 L (see supplementary material). The liquid level was automatically controlled by a vibronic point level detector (Liquiphant FTL31, Endress+Hauser, Switzerland). The synthetic wastewater was introduced at the bottom of each reactors and flowed upwards the granular sludge bed. At the top of the two reactors, supernatant was pumped through a peristaltic pump (Watson Marlow (WMFTG), UK) and recirculated at the lower part to bring additional turbulences and homogenized the dissolved phase. The upflow liquid velocity (ULV) was set around 2 $m.h^{-1}$. A polyethersulfone (PES) flat sheet membrane (Microdyn-Nadir®, Germany) with a nominal pore size of 0.04 µm and a surface area of 0.34 m² was submerged at the center of the one-stage G-AnMBR reactor. The permeate was obtained through a peristaltic pump (LeadFluid®, China) and the net filtration flux was maintained at 1.45 ± 0.35 $L.m^{-2}.h^{-1}$ (LMH). Only an automatic intermittent suction cycle was performed to mitigate membrane fouling at a low energy-demand. The operation cycle was as follows: (i) 8 min 15 s of filtration, (ii) 30 s of initial relaxation, (iii) 45 s of backwash and (iv) 30 s of final relaxation. To get as close as possible to the G-AnMBR configuration and its hydrodynamic pathway, the same membrane module was immersed in the UASB tank but no permeate was suctioned through this membrane. The UASB effluent was pumped through supernatant with the same operation cycle as the G-AnMBR. As shown in Table 1, similar operating conditions were applied in both reactors. The reactors were equipped with temperature sensor, pH and oxidation reduction potential (ORP) probes (PCE Instruments, Deutschland). The physico-chemical

parameters were stable during the campaign and the very low redox (< -450 mV) values confirm that anaerobic conditions were fulfilled. The reactor temperature was kept at around 25°C with a cryostat through a tubular heat exchanger. The hydraulic retention time (HRT) and the OLR were maintained at 13 h and 0.5 $kgCOD.m^{-3}.d^{-1}$. Pressure sensors were installed to monitor atmospheric pressure (Patm), reactors headspace pressures and permeate pressure to obtain the transmembrane pressure (ATM.ECO, Sensor Technik Sirnach (STS), Switzerland). No sludge was intentionally purged except for the need of sampling.

2.3 Analytical methods

DOC was analyzed two days a week on sample pre-filtered at 0.22 µm by TOC analyzer (TOC-V_{CSN}, Shimadzu Corporation, Japan). Mixed liquor suspended solids (MLSS) and mixed liquor volatile suspended solids (MLVSS) were measured weekly in the UASB effluent and G-AnMBR permeate according to Standard Methods (APHA et al., 1998). COD concentrations were determined twice a week using pre-dosed photochemical test (Hach, Germany, LKC 500, 314, 1414, 514) and UV-Vis spectrophotometer (DR3900, Hach, Germany). sCOD was measured after sample filtration through 0.22 µm syringe filter. The denominated tCOD and sCOD removal rates ($tCOD_{removal}$ and $sCOD_{removal}$ respectively) were calculated as follow:

$$tCOD_{removal} = \frac{tCOD_{in} - tCOD_{out}}{tCOD_{in}} = \frac{COD_{removed}}{tCOD_{in}} \quad \text{Eq. 1}$$

$$sCOD_{removal} = \frac{tCOD_{in} - sCOD_{out}}{tCOD_{in}} \quad \text{Eq. 2}$$

where $tCOD_{in}$ is the tCOD measured in the influent, $tCOD_{out}$ is the tCOD of the effluent and $sCOD_{out}$ is the effluent sCOD concentration.

2.4 Three-dimensional fluorescence excitation-emission matrix (3DEEM)

Supernatant from G-AnMBR and effluents from both reactors were pre-filtered through 1.2 µm filter (Grade GF/C, Whatman, UK) and diluted 25 times to limit overlapping signals. The three-dimensional fluorescence excitation-emission matrix (3DEEM) was divided into four areas according to their respective fluorophores and the volume of fluorescence beneath each region were obtained according to Jacquin et al. (2017). The volume of fluorescence (in arbitrary unit per nm² (A.U/nm²)) gives a semi-quantitative information about the amount of fluorophores for each region.

2.5 Granular sludge characteristics

Total solids (TS) and Volatile solids (VS) were measured during reactor seeding according to Standard Methods (APHA et al., 1998). Sludge volume index after 10 minutes (SVI_{10}) and 30 minutes (SVI_{30}) were evaluated by dividing the volume of sludge bed (mL) by the initial sample volume (mL) and the TS concentration of the sample ($gTS.L^{-1}$). The zeta potential of the sludge was measured by Litesizer 500 (Anton Paar, Spaar). The particle size distribution (PSD) of the granular sludge was performed by wet sieving following the method of Derlon et al. (2016) with standard sieves of 0.63 and 0.125 mm mesh sizes. Hence, the sludge was separated into three fractions based on the particle diameter (d_p) such as: (i) large granules with a d_p higher than 0.63 mm ($d_{p \geq 0.63}$), (ii) medium granules mixed with small granules with a dp between 0.63 and 0.125 mm ($d_{p\ 0.125\text{-}0.63}$) and (iii) flocs for the sludge with a dp less than 0.125 mm ($d_{p \leq 0.125}$). TS and VS of each fraction were measured. The proportion of each class of sludge was expressed as percentage of total sludge mass (Eq. 3). VS/TS ratio was calculated within the fractions.

$$Mass\ fraction\_i\ (\%) = \frac{m_i}{\sum_1^3 m_i} \times 100 \qquad \text{Eq. 3}$$

2.6 Methane production

Produced methane was measured in the gas and liquid phases. The gas phase flow rate was continuously recorded by a volumetric flowmeter (MilliGas Counter, Ritter, Germany). Biogas composition of the headspace was regularly analyzed by a gas chromatography system (Clarus 400, Perkin Elmer, USA) coupled with a thermal conductivity detector at 150°C (GC-TCD). Gas phase was collected through a quick gas connection (Swagelok, USA) into an airtight system. 300 µL of the biogas was then sampled through a septum using a gastight syringe (Hamilton Company, USA) and injected into GC-TCD. Methane concentration was defined as the average of all measurements performed during the stable phase of operation. Methane flow rate was converted in NL-CH_4.day^{-1} by using the average temperature and the atmospheric pressure (Patm) of the day. Dissolved methane was quantified based on the headspace method (Giménez et al., 2012; Souza et al., 2011). Vials equipped with a stirrer (total volume (V_T) of 11.6 mL) were sealed with a septum cap and drained with helium during 10 min to avoid any presence of air. A known volume of effluent sample (V_L) was collected using a gastight syringe (Hamilton Company, USA) and injected in sealed vials. Then, vials were kept for stirring at 700 rpm and 25°C for 2h in order to reach gas/liquid equilibrium. Once the equilibrium reached, the total pressure of the headspace (P_T) was recorded and the biogas was analyzed through GC-TCD to determine the methane molar fraction (y_{CH4}). The dissolved methane concentration (C_{CH4}^L) in the effluent was then calculated according to the following expressions:

$$C_{CH4}^L = \frac{C_{CH4}^G \times (V_G + \frac{V_L}{H(T)})}{V_L} \quad \text{Eq. 4}$$

with

$$C_{CH4}^G = \frac{y_{CH4} \times P_T \times MM(CH_4)}{R \times T} \quad \text{Eq. 5}$$

where C_{CH4}^{G} is the CH_4 concentration in the gas phase (mg.L^{-1}), V_G is the volume of the gas phase (L), $MM(CH_4)$ is the molecular weight of methane (16g.mol^{-1}), R is the universal constant of gases (0.082 atm.L.mol^{-1}.K^{-1}), T is the temperature (K) and $H(T)$ is the dimensionless temperature-dependent Henry's constant for methane (Giménez et al., 2012).

The saturation degree was calculated based on the theoretical value of methane dissolved in the liquid phase ($C_{CH4}^{L^*}$, in mg.L^{-1}) calculated according to the Henry's law thermodynamic in equilibrium with the gas phase as described in Eq. 6.

$$Saturation\ degree = \frac{C_{CH4}^{L}}{C_{CH4}^{L^*}} = \frac{C_{CH4}^{L}}{H(T).C_{CH4}^{G}} \quad \text{Eq. 6}$$

2.7 COD mass balance

The COD mass balance was determined based on Eq. 7:

$$tCOD_{in} = tCOD_{out} + COD_{CH4}^{G} + COD_{CH4}^{L} + COD_{SO4} + \Delta COD_{biomass} \quad \text{Eq. 7}$$

where $tCOD_{in}$ and $tCOD_{out}$ are the tCOD measured in the influent and effluent respectively, COD_{CH4}^{G} and COD_{CH4}^{L} correspond to the methane quantified in the gas and liquid phase respectively and converted in equivalent COD using the empirical relationship of 0,38 L-CH_4.gCOD^{-1} at 25°C. COD_{SO4} is the theoretical COD used for sulfate reduction by sulfate-reducing bacteria (SRB) based on the experimental amount of sulfate removal measured and the theoretical value of 0.67 gCOD.gSO_4^{-1}. The residual COD was considered as biomass conversion ($\Delta COD_{biomass}$) and used to calculate the sludge yield (Y_H) of granular biomass as follows :

$$Y_H = \frac{\Delta COD_{biomass}}{1.42\ .\ COD_{removed}} \quad \text{Eq. 8}$$

where Y_H is in gVSS.gCOD$^{-1}_{\text{removed}}$, $\Delta COD_{biomass}$ is in gCOD.day^{-1}, $COD_{removed}$ is in gCOD$_{\text{removed}}$.day^{-1} and 1.42 is the COD to VSS ratio based on the biomass stoichiometry ($C_5H_7O_2N$) (van Lier et al., 2008).

3. Results and discussion

3.1 AnMBR and UASB organic conversion and effluent quality

3.1.1 Organic matter removal

Fig. 1 presents the tCOD and sCOD removal rate in the G-AnMBR and UASB reactors during the overall operation period. Table 2 gives complementary results of the average concentrations of tCOD, sCOD, DOC, MLSS and MLVSS measured in the outlets of both reactors. During the first month of the experiment, the UASB reactor had a very poor tCOD removal efficiency compared to the G-AnMBR reactor which was almost directly stable and efficient (35.9±12.6% and 81.6±3.8% respectively (Table 2)). This difference is clearly due to the UF membrane separation that retains all particles and most of the dissolved and colloidal organic matter (DCOM) in the G-AnMBR whereas small granules, flocs and free-bacteria, just as some DCOM and intermediate degradation products, were washed-out within the supernatant of the UASB (Chen et al., 2017; Ozgun et al., 2015). This can be confirmed by the high amount of MLSS measured in the UASB effluent during the transient period (Table 2) and the same concentration profiles followed by total COD and TSS. As a result, the removal rate for tCOD in the UASB showed an increasing trend until it achieved a steady-state after 31 days of operation. After the transient period, high organic removal efficiencies were carried out in both reactors, as describes in Table 2. Most notably, the G-AnMBR performed higher organic compounds removal (92.3 ± 4.1% of tCOD, 90.0 ± 5.4% of sCOD

246 and 97.8 ± 1.0% of DOC) in comparison to the UASB (79.2 ± 8.5%, 80.7 ± 7.3% and
247 86.5 ± 9.1% of tCOD, sCOD and DOC respectively). This result is well in line with previous
248 studies wherein 40-80% of the tCOD was removed by UASB reactors (Chernicharo et al.,
249 2015) and 71-98% by AnMBR at psychrophilic temperature (see supplementary material).
250 Hence, it appears that the G-AnMBR configuration without gas sparging permits the
251 degradation of organic compounds as high as gas-sparging ones.

252 Relevant differences in sCOD were observed between G-AnMBR supernatant
253 (55.3 ± 16.3 mgCOD.L^{-1}) and sCOD permeate (17.4 ± 4.3 mgCOD.L^{-1}) indicating that a part
254 of soluble compounds does not pass across the membrane. Hence, 16.4 ± 4.7% of the entering
255 sCOD is retained by the membrane barrier and/or removed by the biofilm. The average pore
256 size of the flat sheet membrane is 0.04 µm therefore a part of DCOM (i.e. proteins,
257 polysaccharides, humic aggregates) was expected to be retained by the membrane due to their
258 size. Mechanisms responsible of the retention of the soluble and colloidal matter can be either
259 related to physical phenomenon (i.e. size exclusion, adsorption, charge exclusion) as well as
260 microbial biofilm activity (Smith et al., 2013). Since no COD accumulation was observed in
261 the G-AnMBR supernatant, it can be reasonably assumed that the membrane provides a
262 physical barrier to slowly-biodegradable and non-settleable compounds (e.g. flocs, particles)
263 or by-products (e.g. products from polymers hydrolysis, proteins, SMP) which are later
264 biologically transformed thanks to a longer contact time between bulk sludge and organic
265 material (Gouveia et al., 2015; Ozgun et al., 2015) and thus, explains the enhanced G-
266 AnMBR performances on organic matter removal.

267 Table 3 and Fig. 2 provides complementary information about DCOM behavior inside
268 the anaerobic reactors. Comparing the total volume of fluorescence of the two effluents, it is
269 noticeable that more organics were removed in the G-AnMBR. On average 42.3% of the
270 fluorescent compounds present in the supernatant of the G-AnMBR did not pass through the

membrane. It can be seen from 3DEEM spectra (Fig. 2) and membrane retention rate (Table 3) that protein- and SMP-like molecules (i.e. regions I+II and IV) are the main compounds retained by the submerged membrane. Conversely, humic-like substances (combining fulvic- (III) and humic- (V) acid-like molecules) had the smallest rejection capacity due to their lower molecular weight. No notable increase in total volume of fluorescence was observed in the supernatant of the G-AnMBR over the time. Interestingly, Jacquin et al. (2017) concludes that the protein-like regions are more associated with colloidal proteins whereas the SMP-like are supposed to be macromolecular proteins present in the dissolved phase. These 3DEEM fluorescence results support the substantial benefit of the membrane incorporation inside the anaerobic reactor over the retention and bio-conversion of the macromolecules and colloids. Instead of being taken away with the effluent, like in the UASB, these compounds are kept into the supernatant and could be used as additional organic matter for biogas production.

3.1.2 Suspended solids removal

Concerning the suspended solids removal, nearly all suspended solids (SS) were removed by the membrane filtration (Table 2). In comparison, an average of 10.8 mg/L was found in the UASB effluent during the stable period which is much higher than the G-AnMBR, even if it is under the 35 mgSS.L^{-1} standard regulation discharge (Directive 91/271/EEC). Thus, the results emphasized that UASB combined with UF filtration for DWWT at ambient temperature can achieve an excellent water quality (physical disinfection and suspended matter retention).

3.2 Biogas production

Table 4 presents the results of methane quantification in the gas and the liquid phases. Methane to carbon dioxide ratio of the biogas was around 80/20. This high methane content is a benefit for the energy mass balance and shows a well-functioning of methanogens populations (Chen et al., 2020). The methane flow rate achieved during the steady-state was

296 significantly upper in the G-AnMBR than in the UASB (0.85 ± 0.06 and 0.57 ± 0.05 NL-
297 $CH_4.day^{-1}$ respectively). Interestingly, only a slight difference was observed between methane
298 yields of 0.27 ± 0.03 for the G-AnMBR and 0.22 ± 0.04 L-$CH_4.gCOD_{removed}^{-1}$ for the UASB.
299 This result indicates that no significant improvement in sludge methanogenic activity was
300 observed with the incorporation of a membrane in spite of an increase in global carbon
301 conversion performances (Ozgun et al., 2015). It supports that membrane filtration enhances
302 the net production of methane by retaining particulate matter and DCOM (including VFA).
303 Longer contact time between organics and active biomass allows the conversion of slowly-
304 biodegradable matter and by-products into additional methane.

305 The concentration of methane inside the aqueous phase is about 12.8 mg-$CH_4.L^{-1}$ for the
306 G-AnMBR and 11.8 mg-$CH_4.L^{-1}$ in the UASB, which corresponds approximately to 22% and
307 27% respectively of the total methane produced. Some studies have demonstrated a saturation
308 degree lower in AnMBR than in UASB effluents (Gouveia et al., 2015a). This phenomenon is
309 mainly due to turbulences caused by membrane filtration operating conditions and fouling
310 mitigation technics used that provide a better mixing and so, a better gas-liquid transfer. In
311 this study, the results showed a saturation degree in the G-AnMBR of 2.00 ± 0.10 which is
312 slightly higher than the UASB where the value is 1.80 ± 0.07. Saturation degrees obtained are
313 consistent with Smith et al. (2015) and Souza et al. (2011) results which found oversaturation
314 degrees about 2.2 at 15°C and 1.4-1.7 at 25°C respectively in a UASB treating domestic
315 wastewater. The closeness of the G-AnMBR and UASB values could be explained by the
316 same setup configurations and no fouling control method used aside intermittent filtration.
317 Therefore, no obvious hydrodynamic difference should occur between reactors.

318 By taking into consideration the whole methane generated ($C_{CH4}^{L} + C_{CH4}^{G}$), the methane
319 yields obtained were 0.33 ± 0.03 and 0.28 ± 0.04 NL-CH_4 $gCOD_{removed}^{-1}$ for the G-AnMBR
320 and UASB respectively. The closeness of the average methane yields measured to the

theoretical maximal value (0.38 NL-CH_4.$gCOD_{removed}^{-1}$) demonstrates that an acclimatized biomass could well-convert COD into methane at sub-optimal temperature. Methane yields obtained in this study are in the high-range of the ones conventionally found in anaerobic digestion studies that are mostly between 0.12-0.25 L-CH_4.$gCOD_{removed}^{-1}$. This high conversion rate could be attributed to the long one-year acclimatization of the anaerobic granular sludge at the operating conditions and to the relatively high VFA concentration in the synthetic wastewater that promotes acetogenesis and methanogenesis pathways. Moreover, in this study, the conversion rate takes into account the measured dissolved methane which is generally neglected or estimated through Henry's law coefficient.

3.3 COD mass balance

COD mass balance for the G-AnMBR and UASB are presented in Fig. 3. It is apparent from those results that the G-AnMBR allowed a higher removal rate of the COD since the COD remaining in the UASB effluent is almost three-times higher. The total methane produced by the anaerobic digestion process for the UASB and G-AMBR were 61.1% and 84.7% respectively but only 44.6% and 66.3% were in the gaseous phase and can be directly valuable. This shows the importance to recover dissolved biogas from effluent to avoid environmental issues but also to improve the potential energy recovery. These results are consistent with those obtained by Ji et al. (2021) for an AnMBR pilot-scale treating raw domestic wastewater with close operating conditions (OLR = 0.72 $kgCOD.m^{-3}.d^{-1}$; HRT = 12h ; 25°C) where 10.7% of the COD was remaining in the effluent and 75% of the COD of the influent was converted into methane of which 63% in gaseous phase. It can be seen that the amounts of COD_{in} used for sulfate reduction and the one transformed into dissolved biogas are nearly the same for both anaerobic reactors. This implies that the difference between both methane conversion rate is due to the COD removal capacity and the use of COD_{in} for biomass synthesis.

From the COD entering in the systems, 6.3% (G-AnMBR) and 14.7% (UASB) of the COD were used for biomass production (Fig. 3). This suggests that a higher part of the COD_{in} was consumed for biomass synthesis in the UASB and was therefore not available for methane production. As a result, the calculated sludge yield was about 0.05 $gVSS.gCOD_{removed}^{-1}$ in the G-AnMBR against 0.11 $gVSS.gCOD_{removed}^{-1}$ in the UASB. The sludge yield of the granular biomass corresponds to the typical low anaerobic sludge yield and matches with previous AnMBR studies for DWWT at ambient temperature (see supplementary material). The sludge yield in the UASB was twice higher than the one in the G-AnMBR system. This phenomenon can be explained by the biomass washout occurring in the UASB at the early stage because of the selective hydraulic pressure. According to the Monod equation, the increase of the specific organic loading rate, caused by the loss of flocculated sludge and small granules, stimulates the biomass growth (Chen et al., 2017; Ozgun et al., 2015).

It should be noticed that in the case of AnMBR with external submerged membrane configuration, the selective pressure is not overcome, though, there is an increase in the biomass yield (Chen et al., 2017). Those findings suggest that the G-AnMBR configuration with the membrane submerged inside the mixed granular anaerobic digester enhances the conversion of the COD into methane while maintaining a low sludge production rate. This is of great interest compared to conventional activated sludge processes since the energy requirements as well as the treatment and disposal costs for sludge management could be minimized.

3.4 Granular sludge properties

The settling ability and granulation behavior of the biomass were evaluated through the SVI_{30} and SVI_{10} to SVI_{30} ratio (see supplementary material). Both reactors were inoculated with similar granular sludge SVI of 31.1 and 28.9 $mL.gTS^{-1}$ for UASB and G-AnMBR. Also,

371 the SVI_{10}/SVI_{30} ratio was around 1.3-1.4 meaning that the sludge is a mixture of readily
372 settleable granules and small granules and flocs with a lower capacity of settling. At the end
373 of the operation, SVI_{30} value for the UASB granular sludge decreased sharply (14.7 $mL.gTS^{-1}$)
374 and exhibited a SVI_{10}/SVI_{30} ratio of 1. These results confirm the selective pressure that
375 occurs in the UASB reactor where sole well-settleable granular biomass is kept into the
376 UASB. In contrast, the G-AnMBR configuration does not allow free and flocculated biomass
377 to run-off from the reactor and, as a result, higher SVI_{30} (22.9 $mL.gTS^{-1}$) and SVI_{10}/SVI_{30}
378 ratio (1.3) were measured in comparison to the UASB values.

379 Zeta potential was also measured as it gives an indication about the aptitude of sludge
380 biomass to aggregate among themselves. As suggested by others studies, a higher zeta
381 potential meaning a decline of the negative surface charge and, therefore, electrostatic
382 repulsion could be easily neutralized (Chen et al., 2017). Zeta potential values (see
383 supplementary material) were found higher at the end of the experiment than that at the
384 seeding for the G-AnMBR and UASB reactors suggesting that the biomass attachment has
385 been promoted during process operation.

386 Fig. 4 provides the changing in particle size distribution (PSD) of the granular sludge
387 for both reactors. Seed sludge for UASB and G-AnMBR showed almost identical profiles of
388 PSD corroborating the same inoculation. At the initial stage, large granules ($d_{p \geq 0.63}$)
389 accounted for ≈70% of the total TS mass of the granular sludge whereas the main part of the
390 VS, commonly assimilated to active biomass, belonged to the medium fraction ($d_{p\ 0.125\text{-}0.63}$)
391 with 65 ± 3 % of the total VS mass. As expected, the flocs fraction represented a very low
392 amount of the total biomass since it has a small density compared to granular sludge. After
393 115 days of operation, a significant difference was observed for the granular sludge PSD of
394 the UASB reactor. As expected, shift to larger granules was observed in the UASB reactor
395 with 87.2% and 74.6% of the total TS and VS mass respectively measured in the biggest

396 fraction ($d_{p \geq 0.63}$). This hypothesizes that, besides the sludge washout of poor-settleable
397 particles, growth of larger-sized granules was promoted which is in accordance with the zeta
398 potential values. On the other hand, the granular sludge PSD of the G-AnMBR showed a
399 broader repartition because of the physical barrier retention that permitted the development of
400 various sludge type including free-bacteria and light flocs and granules. As reported in
401 previous studies, a wide variety of biomass (i.e. free-bacteria, fines flocs, granules, cake layer,
402 etc.) results in a large microbial diversity (Lin et al., 2011; Zhou et al., 2019). These results
403 clearly indicate that membrane incorporation enables to maintain the PSD tendency of the
404 granular sludge and leads to a more diversified anaerobic population by allowing the slow
405 growth of anaerobic methanogens (Lin et al., 2013). Moreover, frequent microbial samples
406 were taken during this experiment and will be later analyzed to characterize and confirm the
407 change in diversity and density of the microbial communities following the membrane
408 incorporation. Plus, further experiments should be conducted to evaluate the structural
409 stability of the granules with varying operating conditions to see the range of applicability of
410 the granular biomass.

411 VS/TS ratio depicts in Fig. 4 is an indicator to evaluate the amount of biomass within
412 the granular sludge. A global decrease in VS/TS ratio occurred in UASB intermediate and
413 smaller fractions while the decrease concerned particularly the intermediate granule fraction
414 in the G-AnMBR. This translates an increase in mineral content inside the granular fraction
415 that is exacerbated by biomass loss in the UASB. SEM-EDX analysis provided in
416 supplementary material indicates that the mineral part of the granular sludge was mainly
417 composed of calcium carbonate $CaCO_3$. Prior studies stated that calcium concentration in
418 granules is negatively correlated to VS/TS ratio and bacterial specific activity. Core
419 calcification of granules is a harmful phenomenon as the calcium mineral precipitate and
420 calcium salts deposited in the outer layer limit the diffusion of molecules in granules

421 interstitial spaces (Zhang et al., 2021). It is likely that membrane attenuates the impact of
422 calcification by retaining the flocculated biomass within the reactor which further promote the
423 active biomass inside the granules (i.e. VS/TS ratio).

424 **3.5 G-AnMBR energy recovery evaluation and competitiveness**

425 Based on the methane produced from COD conversion, the energy potentially recovered
426 from DWWT was calculated. Table 5 provides an overview of net energy balance (NEB) and
427 effluent quality for the most common aerobic and anaerobic processes for DWWT at ambient
428 temperature. Anaerobic treatments have an evident energetic advantage comparing to the
429 aerobic DWWT that exhibits a negative NEB from -0.2 to -2 $kWh.m^{-3}$. Although UASB has a
430 low energy demand and high energy recovery (NEB of 0.35-0.5 $kWh.m^{-3}$), the effluent quality
431 obtained is not enough to meet discharge standards and to outcompete CAS or AeMBR
432 reactors (Chernicharo et al., 2015; Ozgun et al., 2013). Conversely, conventional AnMBR
433 reach high organics and suspended solids removal efficiencies but achieve a NEB close to
434 zero due to the gas-sparging energy-demand for membrane fouling control that accounts for
435 more than 70% of the process energy consumption (Smith et al., 2014). Therefore, it is
436 apparent from Table 5 that the G-AnMBR operated in this study is the only system which
437 allows both excellent effluent quality and strong positive net energy balance, even when the
438 dissolved methane is not recovered (0.58 $kWh.m^{-3}$). This finding highlights the interest of the
439 G-AnMBR submerged configuration with no gas-sparging fouling control which optimizes at
440 the same time COD to methane conversion rate, energy-requirement, effluent quality and
441 reactor compactness. Hence, G-AnMBR technologies could be useful in poor-energy, water-
442 shortage and scarce-space areas (Kong et al., 2021a; Robles et al., 2018). In addition,
443 considering the complete recovery of dissolved biogas, nearly 0.20 $kWh.m^{-3}$ of additional
444 energy could be generated from the domestic WW by G-AnMBR treatment. As mentioned
445 above, it points out that the dissolved methane recovery needs further investigation as it

accounts for more than 25% of the total produced methane and because methane is an important greenhouse concern (Gouveia et al., 2015; Ji et al., 2021; Smith et al., 2013).

Conclusion

It has been demonstrated that the submerged G-AnMBR configuration, without gas sparging, represents a sustainable biotechnology for DWWT at ambient temperatures over conventional processes with regard to effluent quality and energy requirements. The membrane barrier helped to maintain the process stability, led to a broader sludge diversity with no granular sludge activity alteration. The G-AnMBR reached organic removal rate as high as aerobic process with a tCOD removal of ~92.3%. The NEB was maximized to +0.58 $kWh.m^{-3}$ with the G-AnMBR setup without gas-sparging, bringing the G-AnMBR as a promising process which may be part of the circular economy strategies.

Acknowledgments

This work was supported by a grant overseen by the French National Research Agency as part of the "JCJC" Program BàMAn (ANR-18-CE04-0001-01). Special thanks are addressed to Patrice Montels and Daniel Valenza (IEM) for the pilot design and building and Didier Cot and Bertrand Rebière (IEM) for the SEM-EDX analysis.

References

APHA, AWWA, WEF (Eds.), 1998. Standard methods: for the examination of water and wastewater, 20. ed. ed. American Public Health Association, Washington, DC.

Batstone, D.J., Virdis, B., 2014. The role of anaerobic digestion in the emerging energy economy. Current Opinion in Biotechnology, Energy biotechnology • Environmental biotechnology 27, 142–149.

Chen, C., Guo, W., Ngo, H.H., 2016. Advances in Granular Growth Anaerobic Membrane Bioreactor (G-AnMBR) for Low Strength Wastewater Treatment 7.

Chen, C., Guo, W., Ngo, H.H., Chang, S.W., Duc Nguyen, D., Dan Nguyen, P., Bui, X.T., Wu, Y., 2017. Impact of reactor configurations on the performance of a granular anaerobic membrane bioreactor for municipal wastewater treatment. International Biodeterioration & Biodegradation 121, 131–138.

Chen, C., Liu, Z., Huang, X., 2020. 14 - Anaerobic membrane bioreactors for sustainable and energy-efficient municipal wastewater treatment, in: Ngo, H.H., Guo, W., Ng, H.Y., Mannina, G., Pandey, A. (Eds.), Current Developments in Biotechnology and Bioengineering. Elsevier, pp. 335–366.

Chen, R., Nie, Y., Ji, J., Utashiro, T., Li, Q., Komori, D., Li, Y., 2017. Submerged anaerobic membrane bioreactor (SAnMBR) performance on sewage treatment: removal efficiencies, biogas production and membrane fouling. Water science and technology 76, 1308–1317.

Chernicharo, C.A.L., van Lier, J.B., Noyola, A., Bressani Ribeiro, T., 2015. Anaerobic sewage treatment: state of the art, constraints and challenges. Rev Environ Sci Biotechnol 14, 649–679.

Deng, L., Guo, W., Ngo, H.H., Zhang, J., Liang, S., 2020. Advanced anaerobic membrane bioreactors: Performance enhancers and their hybrid systems, in: Ngo, H.H., Guo, W., Ng, H.Y., Mannina, G., Pandey, A. (Eds.), Current Developments in Biotechnology and Bioengineering. Elsevier, pp. 109–142.

Derlon, N., Wagner, J., da Costa, R.H.R., Morgenroth, E., 2016. Formation of aerobic granules for the treatment of real and low-strength municipal wastewater using a sequencing batch reactor operated at constant volume. Water Research 105, 341–350.

Giménez, J.B., Martí, N., Ferrer, J., Seco, A., 2012. Methane recovery efficiency in a submerged anaerobic membrane bioreactor (SAnMBR) treating sulphate-rich urban wastewater: Evaluation of methane losses with the effluent. Bioresource Technology 118, 67–72.

Gouveia, J., Plaza, F., Garralon, G., Fdz-Polanco, F., Peña, M., 2015. A novel configuration for an anaerobic submerged membrane bioreactor (AnSMBR). Long-term treatment of municipal wastewater under psychrophilic conditions. Bioresource Technology 198, 510–519.

Iorhemen, O.T., Hamza, R.A., Tay, J.H., 2017. Membrane fouling control in membrane bioreactors (MBRs) using granular materials. Bioresource Technology, Special issue on Challenges in Environmental Science and Engineering, CESE-2016 240, 9–24.

Jacquin, C., Lesage, G., Traber, J., Pronk, W., Heran, M., 2017. Three-dimensional excitation and emission matrix fluorescence (3DEEM) for quick and pseudo-quantitative determination of protein- and humic-like substances in full-scale membrane bioreactor (MBR). Water Res 118, 82–92.

Ji, J., Ni, J., Ohtsu, A., Isozumi, N., Hu, Y., Du, R., Chen, Y., Qin, Y., Kubota, K., Li, Y.-Y., 2021. Important effects of temperature on treating real municipal wastewater by a submerged anaerobic membrane bioreactor: Removal efficiency, biogas, and microbial community. Bioresour Technol 336, 125306.

511 Jones, E.R., van Vliet, M.T.H., Qadir, M., Bierkens, M.F.P., 2021. Country-level and
512 gridded estimates of wastewater production, collection, treatment and reuse. Earth System
513 Science Data 13, 237–254.

514 Kong, Z., Li, L., Wu, J., Wang, T., Rong, C., Luo, Z., Pan, Y., Li, D., Li, Y., Huang, Y.,
515 Li, Y.-Y., 2021a. Evaluation of bio-energy recovery from the anaerobic treatment of
516 municipal wastewater by a pilot-scale submerged anaerobic membrane bioreactor (AnMBR)
517 at ambient temperature. Bioresource Technology 339, 125551.

518 Kong, Z., Wu, J., Rong, C., Wang, T., Li, L., Luo, Z., Ji, J., Hanaoka, T., Sakemi, S., Ito,
519 M., Kobayashi, S., Kobayashi, M., Qin, Y., Li, Y.-Y., 2021b. Large pilot-scale submerged
520 anaerobic membrane bioreactor for the treatment of municipal wastewater and biogas
521 production at 25 °C. Bioresour Technol 319, 124123.

522 Layer, M., Adler, A., Reynaert, E., Hernandez, A., Pagni, M., Morgenroth, E., Holliger,
523 C., Derlon, N., 2019. Organic substrate diffusibility governs microbial community
524 composition, nutrient removal performance and kinetics of granulation of aerobic granular
525 sludge. Water Research X 4, 100033.

526 Liao, B.-Q., Kraemer, J.T., Bagley, D.M., 2006. Anaerobic Membrane Bioreactors:
527 Applications and Research Directions. Critical Reviews in Environmental Science and
528 Technology 36, 489–530.

529 Lin, H., Peng, W., Zhang, M., Chen, J., Hong, H., Zhang, Y., 2013. A review on
530 anaerobic membrane bioreactors: Applications, membrane fouling and future perspectives.
531 Desalination 314, 169–188.

Lin, H.J., Gao, W.J., Leung, K.T., Liao, B.Q., 2011. Characteristics of different fractions of microbial flocs and their role in membrane foulingH. J. Lin et al.Characteristics of different fractions of microbial flocs in membrane fouling. Water Sci Technol 63, 262–269.

Lobato, L.C.S., Chernicharo, C.A.L., Souza, C.L., 2012. Estimates of methane loss and energy recovery potential in anaerobic reactors treating domestic wastewater. Water Science and Technology 66, 2745–2753.

Maaz, M., Yasin, M., Aslam, M., Kumar, G., Atabani, A.E., Idrees, M., Anjum, F., Jamil, F., Ahmad, R., Khan, A.L., Lesage, G., Heran, M., Kim, J., 2019. Anaerobic membrane bioreactors for wastewater treatment: Novel configurations, fouling control and energy considerations. Bioresource Technology 283, 358–372.

Ozgun, H., Dereli, R.K., Ersahin, M.E., Kinaci, C., Spanjers, H., van Lier, J.B., 2013. A review of anaerobic membrane bioreactors for municipal wastewater treatment: Integration options, limitations and expectations. Separation and Purification Technology 118, 89–104.

Ozgun, H., Gimenez, J.B., Ersahin, M.E., Tao, Y., Spanjers, H., van Lier, J.B., 2015. Impact of membrane addition for effluent extraction on the performance and sludge characteristics of upflow anaerobic sludge blanket reactors treating municipal wastewater. Journal of Membrane Science 479, 95–104.

Robles, Á., Ruano, M.V., Charfi, A., Lesage, G., Heran, M., Harmand, J., Seco, A., Steyer, J.-P., Batstone, D.J., Kim, J., Ferrer, J., 2018. A review on anaerobic membrane bioreactors (AnMBRs) focused on modelling and control aspects. Bioresource Technology 270, 612–626.

553 Roccaro, P., Vagliasindi, F.G.A., 2020. Membrane bioreactors for wastewater
554 reclamation: Cost analysis, in: Current Developments in Biotechnology and Bioengineering.
555 Elsevier, pp. 311–322.

556 Safitri, A.S., Hamelin, J., Kommedal, R., Milferstedt, K., 2021. Engineered
557 methanotrophic syntrophy in photogranule communities removes dissolved methane. Water
558 Research X 12, 100106.

559 Smith, A.L., J. Skerlos, S., Raskin, L., 2015. Anaerobic membrane bioreactor treatment
560 of domestic wastewater at psychrophilic temperatures ranging from 15 °C to 3 °C.
561 Environmental Science: Water Research & Technology 1, 56–64.

562 Smith, A.L., Skerlos, S.J., Raskin, L., 2013. Psychrophilic anaerobic membrane
563 bioreactor treatment of domestic wastewater. Water Research 47, 1655–1665.

564 Smith, A.L., Stadler, L.B., Cao, L., Love, N.G., Raskin, L., Skerlos, S.J., 2014.
565 Navigating Wastewater Energy Recovery Strategies: A Life Cycle Comparison of Anaerobic
566 Membrane Bioreactor and Conventional Treatment Systems with Anaerobic Digestion.
567 Environ. Sci. Technol. 48, 5972–5981.

568 Sohaib, Q., Kalakech, C., Charmette, C., Cartier, J., Lesage, G., Mericq, J.-P., 2022.
569 Hollow-Fiber Membrane Contactor for Biogas Recovery from Real Anaerobic Membrane
570 Bioreactor Permeate. Membranes 12, 112.

571 Souza, C.L., Chernicharo, C.A.L., Aquino, S.F., 2011. Quantification of dissolved
572 methane in UASB reactors treating domestic wastewater under different operating conditions.
573 Water Sci Technol 64, 2259–2264.

574 Srinivasa Raghavan, D.S., Qiu, G., Song, Y., Ting, Y.-P., 2017. Anaerobic Treatment of
575 Low-Strength Wastewater, in: Current Developments in Biotechnology and Bioengineering.
576 Elsevier, pp. 293–320.

577 Su, X., Chiang, P., Pan, S., Chen, G., Tao, Y., Wu, G., Wang, F., Cao, W., 2019.
578 Systematic approach to evaluating environmental and ecological technologies for wastewater
579 treatment. Chemosphere 218, 778–792.

580 van Lier, J.B., Mahmoud, N., Zeeman, G., 2008. Anaerobic Wastewater Treatment, in:
581 Biological Wastewater Treatment: Principles, Medelling and Design. IWA Publishing.

582 Vinardell, S., Astals, S., Peces, M., Cardete, M.A., Fernández, I., Mata-Alvarez, J.,
583 Dosta, J., 2020. Advances in anaerobic membrane bioreactor technology for municipal
584 wastewater treatment: A 2020 updated review. Renewable and Sustainable Energy Reviews
585 130, 109936.

586 Zhang, J., Pan, J.-Q., Zhao, S., Gan, P., Qin, C.-R., Wang, Z.-W., Chen, Y., Liu, X., Lu,
587 L.-H., Wang, S.-F., 2021. Calcium migration inside anaerobic granular sludge: Evidence from
588 calcium carbonate precipitation pattern. Colloids and Surfaces A: Physicochemical and
589 Engineering Aspects 625, 126890.

590 Zhou, Z., Tao, Y., Zhang, S., Xiao, Y., Meng, F., Stuckey, D.C., 2019. Size-dependent
591 microbial diversity of sub-visible particles in a submerged anaerobic membrane bioreactor
592 (SAnMBR): Implications for membrane fouling. Water Research 159, 20–29.

593 Table 1 - G-AnMBR and UASB operating conditions (mean values ± SD).

Parameter	G-AnMBR	UASB
Temperature (°C)	25.0 ± 0.8	25.8 ± 1.8
pH (-)	7.0 ± 0.2	7.1 ± 0.2
Redox (mV)	-462 ± 37	-456 ± 32
$Jp_{20,NET}$ (LMH)	1.34 ± 0.14	-
$Jp_{20,INST}$	2.48 ± 0.22	-
HRT (h)	13.1 ± 2.0	13.2 ± 3.0
OLR ($kgCOD.m^{-3}.d^{-1}$)	0.50 ± 0.14	0.48 ± 0.15
ULV ($m.h^{-1}$)	2.25	2.04

594

595 Table 2 - Effluent composition and removal efficiencies of the G-AnMBR and UASB (mean values ± SD ;
596 $n \geq 20$).

		G-AnMBR permeate		UASB effluent	
Phase		Transient	Steady	Transient	Steady
$tCOD_{eff}$	(mg/L)	43.3 ± 13.1	22.0 ± 14.5	150.2 ± 36.0	59.0 ± 28.5
$tCOD_{removal}$	(%)	81.6 ± 3.8	92.3 ± 4.1	35.9 ± 12.6	79.2 ± 8.5
$sCOD_{eff}$	(mg/L)	43.3 ± 13.1	22.0 ± 14.5	69.0 ± 8.1	44.1 ± 18.9
$sCOD_{removal}$	(%)	76.7 ± 3.6	90.0 ± 5.4	63.9 ± 7.8	80.7 ± 7.3
DOC_{eff}	(mg/L)	7.5 ± 0.0	2.1 ± 0.6	23.6 ± 0.0	13.8 ± 9.4
$DOC_{removal}$	(%)	85.7 ± 0.0	97.8 ± 1.0	60.0 ± 0.0	86.5 ± 9.1
$MLSS_{eff}$	(mg/L)	ND	ND	113.1 ± 87.7	10.8 ± 6.0
$MLVSS_{eff}$	(mg/L)	ND	ND	60.4 ± 37.4	9.3 ± 5.4

597 ND : non-detectable

598

599 Table 3 - Average normalized volume of fluorescence for the different regions of the 3DEEM spectra for G-
600 AnMBR supernatant and permeate and UASB effluent and the membrane rejection during the steady-state
601 period. Errors represent standard deviation (n=7).

		3DEEM Region			
		I+II	IV	III+V	Total
G-AnMBR	Supernatant ($\times 10^8$ A.U/nm²)	2.74 ± 1.04	0.12 ± 0.03	0.52 ± 0.09	3.38 ± 1.10
	Permeate ($\times 10^8$ A.U/nm²)	1.46 ± 0.68	0.05 ± 0.01	0.40 ± 0.07	1.90 ± 0.69
	Membrane rejection (%)	45.9 ± 20.0	59.8 ± 18.3	24.0 ± 14.6	42.3 ± 17.6
UASB	Effluent ($\times 10^8$ A.U/nm²)	2.45 ± 1.40	0.12 ± 0.08	0.45 ± 0.14	3.02 ± 1.59

602

603 Table 4 - Methane production in the gas phase and liquid phase (mean values ± SD ; n ≥ 15).

	Unit	G-AnMBR	UASB
CH_4 flow rate	$NL\text{-}CH_4.day^{-1}$	0.85 ± 0.06	0.57 ± 0.05
CH_4/CO_2 ratio	% / %	79.9/20.1 ± 3.5	81.9/18.1 ± 6.8
Gaseous methane yield	$NL\text{-}CH_4/g\text{-}COD_{removed}$	0.27 ± 0.03	0.22 ± 0.04
Dissolved methane	$mg\text{-}CH_4.L^{-1}$	12.8 ± 0.7	11.7 ± 1.1
Degree of saturation	-	2.00 ± 0.10	1.80 ± 0.07
Dissolved CH_4 flow rate	$NL\text{-}CH_4.day^{-1}$	0.24 ± 0.01	0.22 ± 0.02
Total methane yield	$NL\text{-}CH_4/g\text{-}COD_{removed}$	0.33 ± 0.03	0.28 ± 0.04

604

605 Table 5 - Comparison of net energy balance and effluent quality between aerobic and anaerobic technologies for
606 low-strenght domestic wastewater treatment at ambient temperature (≤25°C).

				Effluent quality	
	Energy consumption	Energy from CH_4	Net Energy Balance	COD removal	Effluent TSS
	($kWh.m^{-3}$)	($kWh.m^{-3}$)	($kWh.m^{-3}$)	(%)	($mg.L^{-1}$)
CAS	0.2 – 0.8 [a,b]	-	-0.2 – -0.8	85-93 [a]	<30
AeMBR	0.6 – 2 [b,c]	-	-0.6 – -2	>95 [a]	<1[c]
UASB	0.11[d]	0.6 [d]	0.5	40-80 [g,h]	60-200 [h]
		0.46 (0.64*) [j]	0.35 (0.53*)	79 [j]	≅ 10 [j]
AnMBR	0.3 – 0.5 [e,f]	0.3 – 0.4 [e,f]	-0.1 – 0.1	>80-90 [i]	<1[h,i]
G-AnMBR	0.12 [j]	0.70 (0.89*) [j]	0.58 (0.77*)	92 [j]	<1 [j]
				>90 [i]	

607 a. (Su et al., 2019) ; b. (Roccaro and Vagliasindi, 2020) ; c. (Liao et al., 2006) ; d. (Lobato. Chernicharo. et
608 Souza 2012) ; e. (Kong et al., 2021a) ; f. (Smith et al., 2014) ; g. (van Lier et al., 2008) ; h. (Chernicharo et al.,
609 2015) ; i. (Chen et al., 2020) ; j. This study.
610 (_*) Those values in brackets take into account the complete dissolved methane recovery.
611 MBR values are for submerged membrane configuration.

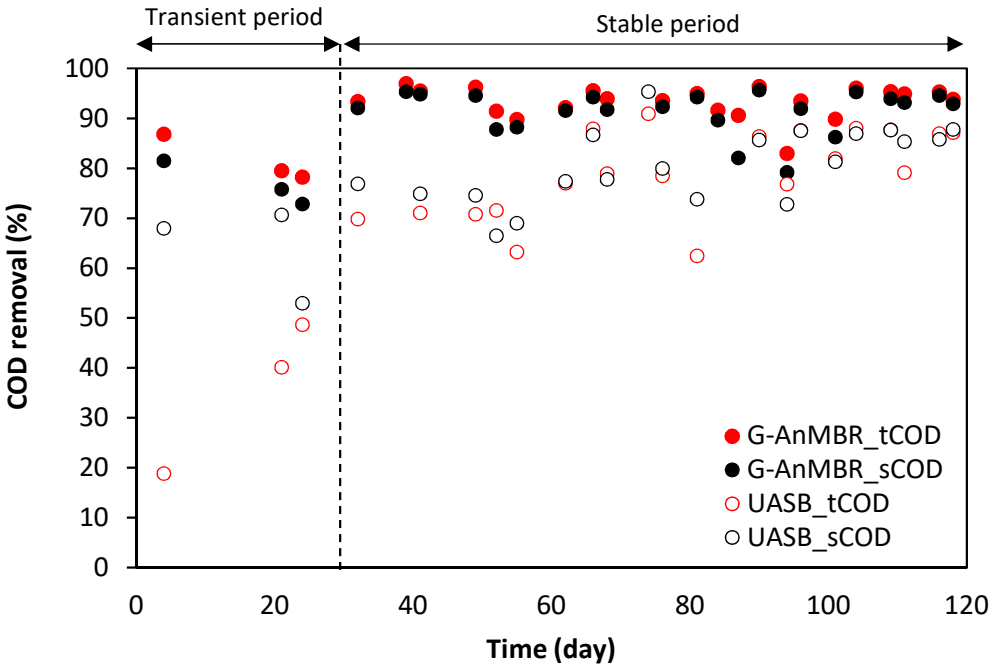

Fig. 1 - Total and soluble COD removal efficiencies in the UASB effluent and AnMBR permeate during the 120 days of operation.

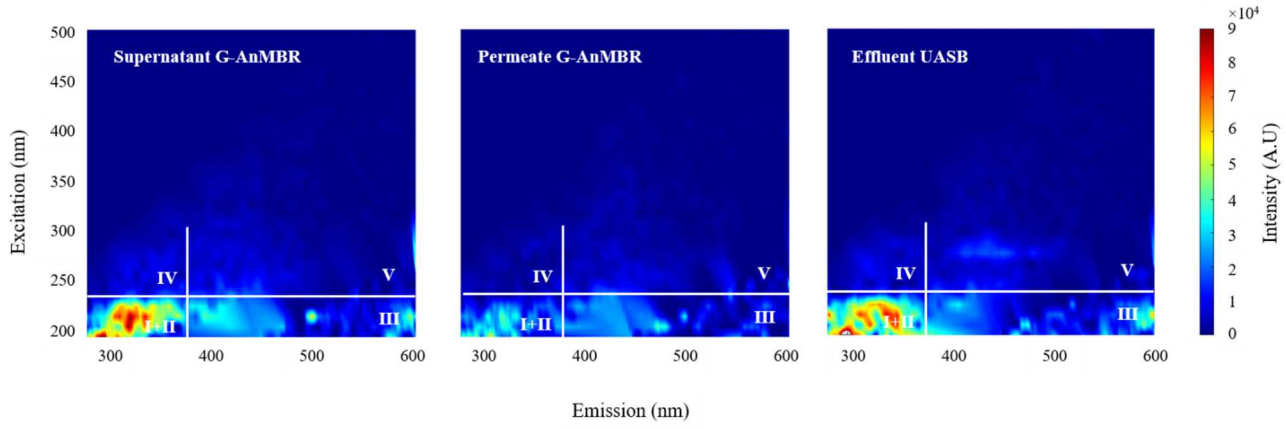

Fig. 2 - 3DEEM fluorescence spectra of G-AnMBR supernatant and permeate and UASB effluent on day 94

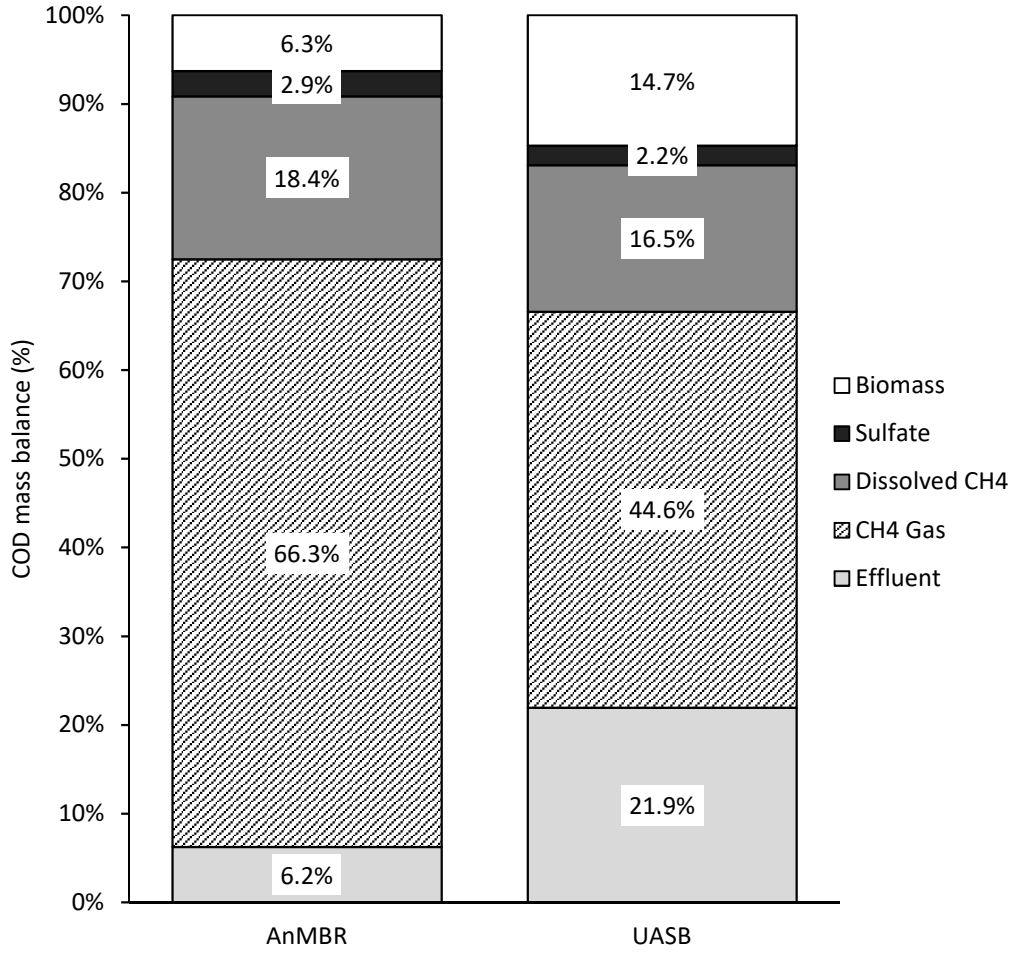

Fig. 3 - Average COD mass balance in the UASB and G-AnMBR reactors during the steady-state period (from day 30 to 120).

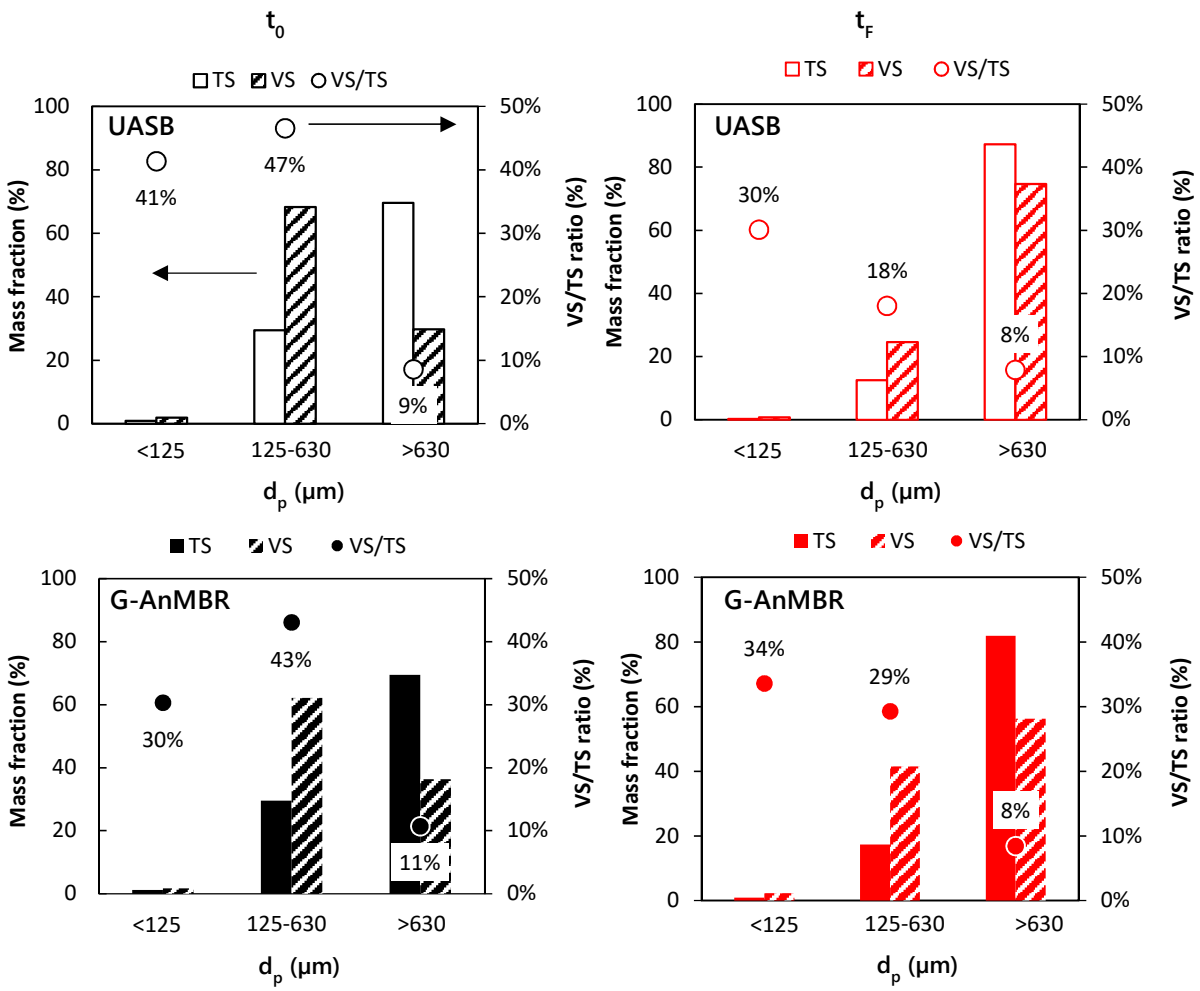

Fig. 4- Particle size distribution of the UASB and G-AnMBR granular sludge at the beginning (t_0 = day 1) and at the end (t_F = day 115) of the experiment.

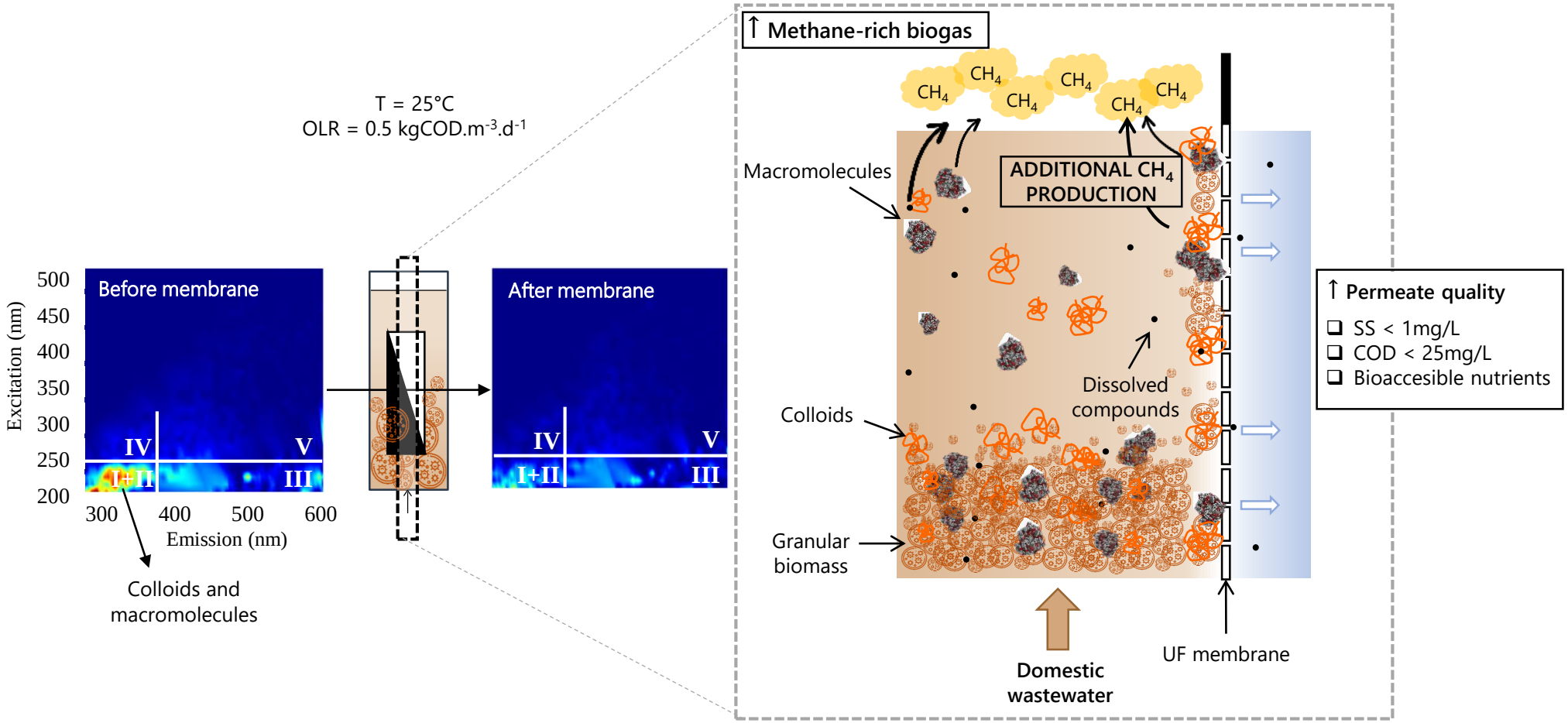
T = 25°C
OLR = 0.5 kgCOD.m-3.d-1
Before membrane
After membrane
Excitation (nm)
Emission (nm)
IV
V
I+II
III
Colloids and macromolecules
↑ Methane-rich biogas
CH4
Macromolecules
ADDITIONAL CH4 PRODUCTION
Dissolved compounds
Colloids
Granular biomass
Domestic wastewater
UF membrane
↑ Permeate quality
SS < 1mg/L
COD < 25mg/L
Bioaccesible nutrients